Journal of Applied Physics

Insulating improper ferroelectric domain walls as robust barrier layer capacitors

Cite as: J. Appl. Phys. **129**, 074101 (2021); https://doi.org/10.1063/5.0038300
Submitted: 20 November 2020 • Accepted: 28 December 2020 • Published Online: 16 February 2021

Lukas Puntigam, Jan Schultheiß, Ana Strinic, et al.

AIP Publishing

Journal of Applied Physics ARTICLE scitation.org/journal/jap

Insulating improper ferroelectric domain walls as robust barrier layer capacitors

Cite as: J. Appl. Phys. **129**, 074101 (2021); doi: 10.1063/5.0038300
Submitted: 20 November 2020 · Accepted: 28 December 2020 ·
Published Online: 16 February 2021

View Online Export Citation CrossMark

Lukas Puntigam,[1] Jan Schultheiß,[2] Ana Strinic,[1] Zewu Yan,[3,4] Edith Bourret,[3] Markus Altthaler,[1] István Kézsmárki,[1] Donald M. Evans,[1,2] Dennis Meier,[2] and Stephan Krohns[1,a)]

AFFILIATIONS

[1]Experimental Physics V, Center for Electronic Correlations and Magnetism, Institute of Physics, University of Augsburg, 86135 Augsburg, Germany
[2]Department of Materials Science and Engineering, Norwegian University of Science and Technology (NTNU), 7043 Trondheim, Norway
[3]Materials Sciences Division, Lawrence Berkeley National Laboratory, Berkeley, California 94720, USA
[4]Department of Physics, ETH Zurich, 8093 Zürich, Switzerland

Note: This paper is part of the Special Topic on Domains and Domain Walls in Ferroic Materials.
a)Author to whom correspondence should be addressed: stephan.krohns@physik.uni-augsburg.de

ABSTRACT

We report the dielectric properties of improper ferroelectric hexagonal (h-)$ErMnO_3$. From the bulk characterization, we observe a temperature and frequency range with two distinct relaxation-like features, leading to high and even "colossal" values for the dielectric permittivity. One feature trivially originates from the formation of a Schottky barrier at the electrode–sample interface, whereas the second one relates to an internal barrier layer capacitance (BLC). The calculated volume fraction of the internal BLC (of 8%) is in good agreement with the observed volume fraction of insulating domain walls (DWs). While it is established that insulating DWs can give rise to high dielectric constants, studies typically focused on proper ferroelectrics where electric fields can remove the DWs. In h-$ErMnO_3$, by contrast, the insulating DWs are topologically protected, facilitating operation under substantially higher electric fields. Our findings provide the basis for a conceptually new approach to engineer materials exhibiting colossal dielectric permittivities using domain walls in improper ferroelectrics.

I. INTRODUCTION

Materials exhibiting very high values in dielectric permittivity ($\varepsilon' > 10^3$) are often coined as "colossal dielectric constant" (CDC) materials.[1,2] They bear enormous potential for enhancing the capacitance, e.g., in multilayer ceramic or low-temperature co-fired capacitors.[3–5] Typically, proper ferroelectric materials,[6] such as $BaTiO_3$,[7,8] or $Pb(Zr_x,Ti_{1-x})O_3$,[9] are used as their dielectric permittivity exceeds 10^3 at ambient temperatures and the loss tangent—indicating the dielectric loss—is rather low ($\tan\delta < 10^{-2}$).[4,10,11] The frequency stabilities of these parameters within a certain temperature range with respect to the applied voltages are key quantities for technical applicability.

Another approach toward CDCs is to use thin layers with reduced conductivity—so-called barrier layer capacitances (BLCs)—in bulk ceramics and single crystals. These BLCs can be internal layers, like insulating grain boundaries in polycrystalline ceramics,[12–14] or surface layers formed, e.g., due to the depletion zone of Schottky diodes arising at metal–semiconductor contacts.[15,16] Both mechanisms are sensitive to variations in preparation (i.e., size of grains and conductivity of grain boundaries[13]) or the contact area of the Schottky barrier. BLCs appear as a step-like decrease in ε' accompanied by a peak in ε'' in a frequency-dependent representation mimicking a classical "Debye-like" relaxation process (see Lunkenheimer *et al.*[1] and references therein for more details). The electrical heterogeneity is responsible for the first relaxation-like feature in the dielectric properties, called the Maxwell–Wagner relaxation.

Recently, a reduced conductivity at the domain walls (DWs) and a related BLC effect were observed in h-$YMnO_3$,[17] suggesting a high dielectric constant $\varepsilon' > 200$. However, a systematic analysis

that can confirm the connection between the high dielectric constant and DW driven BLCs remains illusive.

Here, we provide a dielectric analysis of an h-$ErMnO_3$ single crystal for which the polarization is parallel to the applied contact electrodes (in-plane). Two distinct relaxations are observed in this sample: the first leads to a high dielectric constant of the order of 300 and the second to a CDC of more than 5×10^3. So far, mainly the dielectric properties of out-of-plane polarized samples were investigated, for which often only one relaxation was reported leading to CDC.[18–20] To disentangle the contribution of various BLCs arising in the sample and at the surface of the sample, we simulate the dielectric spectra by an equivalent circuit model, analogous to previous studies on the CDC prime-example, $CaCu_3Ti_4O_{12}$.[1,2,21] This approach, in combination with a distinct modification of the electrode contact area and the thickness of the sample, allows us to distinguish BLCs arising from internal and surface effects. Furthermore, we use local-probe analysis by piezo-force response (PFM) and conductive atomic force microscopy (cAFM) to determine the electronic DW properties at the sample surface and estimate the volume fraction of insulating DW.[22,23] Our systematic analysis provides new insight into the dielectric properties of hexagonal manganites, corroborating that insulating DWs act as BLCs, playing a key role for the high or even colossal dielectric constants observed in this class of materials.

II. EXPERIMENT

High-quality hexagonal h-$ErMnO_3$ single crystals were grown by the pressurized floating zone technique.[24] The sample was cut into a disk (area = 2.38 mm^2, thickness = 0.61 mm) with the polar axis lying parallel to the surface, i.e., (110)-oriented. For dielectric spectroscopy, we used a plate capacitor geometry, coating both top and bottom surfaces either with silver paint or sputtered gold. We performed the measurements using an Alpha Analyzer (Novocontrol, Montabaur, Germany), which covers the frequency range of 1 Hz to 1 MHz. This analysis was conducted in a closed-cycle refrigerator between 150 K and 300 K.

The microscopic data were recorded on the same sample at room temperature using an NT-MDT (NTEGRA, Apeldoorn, Netherlands) atomic force microscope (AFM), using diamond tips (DDESP-10, Bruker, Billerica, MA, USA). The sample was lapped with a 9 μm-grained Al_2O_3 water suspension and polished using silica slurry (Ultra-Sol® 2EX, Eminess Technologies, Scottsdale, AZ, USA) to produce a flat surface with a root mean square (RMS) roughness of about 1.65 nm (determined over a $25 \times 25\,\mu m^2$ area). For domain imaging by PFM, an ac-excitation voltage of 10 V was applied to the back electrode at a frequency of 61 kHz while the tip was grounded. Local transport data were gained by cAFM with a dc-voltage of 2 V applied to the back electrode.

III. RESULTS AND DISCUSSION

A. Two relaxation-like dielectric features

Figure 1 shows the temperature-dependent dielectric constant ε' (a) and loss tangent $\tan\delta$ (b) for various frequencies from 1 Hz to 1 MHz. The electrodes were made with silver paint. For almost

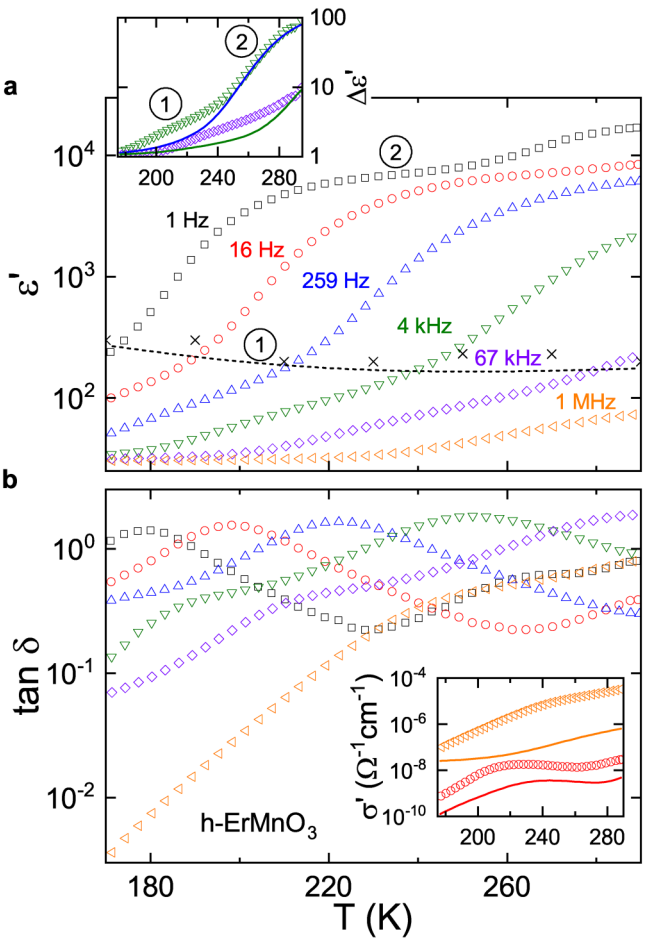

FIG. 1. Temperature-dependence of ε' (a) and $\tan\delta$ (b) of h-$ErMnO_3$ with in-plane polarization at selected frequencies from 1 Hz to 1 MHz. The inset in (a) compares $\Delta\varepsilon' = \varepsilon'/\varepsilon_\infty$ of samples with in-plane (open symbols) and out-of-plane (lines) polarization cut from the same batch for two different frequencies [colors refer to the respective frequencies in (a)]. The data for the out-of-plane sample were taken from Ruff *et al.*[19] Numbers (① and ②) indicate the relaxation-like features; the black crosses (fit parameters of the equivalent circuit analysis from Table S1 in the supplementary material) and the dashed line give a guide to the eye for the temperature-dependency of the lower feature. The inset in (b) compares the temperature-dependent conductivity σ' for these samples for two frequencies [again, colors refer to the respective frequencies in (a)].

all frequencies, ε' exhibits a distinct two-step increase from about 30 to 200–400 and further to $\varepsilon' > 5 \times 10^3$. These steps in ε' are accompanied by a peak in $\tan\delta$, e.g., for the 4 kHz curve at about 185 K and 255 K, respectively. This behavior corresponds to a relaxation process in the temperature-dependent representation. Such prominent relaxation-like features are well known in oxide materials,[1] often originating from BLCs, e.g., Schottky diodes forming a depletion zone that acts as a thin insulating layer. Further, the rather high values of the loss tangent ($\tan\delta > 0.01$) corroborate

the framework of BLC mechanisms responsible for the dielectric features. However, compared to other BLC materials, e.g., $CaCu_3Ti_4O_{12}$[25] or $La_{15/8}Sr_{1/8}NiO_4$,[16] the loss tangent of the lower dielectric feature of the investigated h-$ErMnO_3$ is reduced.

Recently, it was reported that in h-$YMnO_3$ and h-$ErMnO_3$, Schottky barriers give rise to CDCs.[17–20] Similar to this work (Fig. 1), two distinct relaxation-like features on h-$YMnO_3$ were measured;[17] one attributed to an internal BLC mechanism, possibly originating from insulating DWs. In contrast to the previously published data gained on samples with out-of-plane polarization, the measurements presented in Fig. 1 show well separated features, facilitating a more detailed analysis. We illustrate this difference in the inset in Fig. 1(a), comparing the change in dielectric constant $\Delta\varepsilon'$ for the present in-plane oriented sample to an out-of-plane oriented one, published in Ruff *et al.*[19] The CDC feature ② is the same for both orientations, while the high dielectric constant feature ① appears as a distinct increase only for the in-plane sample. It is important to note that for this comparison of ε' we used different frequencies for the in-plane (259 Hz and 4 kHz) and out-of-plane (4 kHz and 67 kHz) orientation. For BLC-driven mechanisms, the bulk dc-conductivity has a strong impact on the temperature and frequency range, where this feature dominates the dielectric properties.[1] The inset of Fig. 1(b) shows σ' for two representative frequencies, indicating a significant decrease of the conductivity of the out-of-plane oriented sample corroborating the above mentioned shift in the BLC-driven feature. This is confirmed by the frequency-dependent dielectric analysis of h-$(Er_{0.99}Ca_{0.01})MnO_3$ shown in Fig. S1 in the supplementary material. This is the first hint of an anisotropic BLC feature, which is either based on the change in dc-conductivity or might be due to differences in DW density or conductance. For the latter, it is already well established via local-probe measurements that the conductance of the DWs strongly depends on the orientation of the polarization.[22,26]

B. Quantifying the DW density

We use PFM and cAFM to estimate the density of DWs, which provide a possible origin for the observed high dielectric constant feature.

To approximate the density of these DWs in our h-$ErMnO_3$ crystal, we map the domain distribution at the sample surface using PFM (in-plane contrast) as presented in Fig. 2(a). The PFM scan reveals the typical domain distribution, characteristic for hexagonal manganites.[27–29] To determine the domain/DW density, we evaluate multiple test lines [one line is shown in Fig. 2(b) and further lines in Fig. S3 in the supplementary material] applying the procedure outlined in the textbook by Hubert and Schäfer.[30] Measurements by cAFM [Fig. 2(c)] confirm the presence of DWs with enhanced (tail-to-tail) and reduced (head-to-head) conductance.[22] From this analysis, we find 1 ± 0.1 DWs per μm with enhanced or reduced conductance in comparison to the domains. The same evaluation was also performed for h-$(Er_{0.99}Ca_{0.01})MnO_3$ depicted in Fig. S2 in the supplementary material, providing a similar domain/DW fraction.

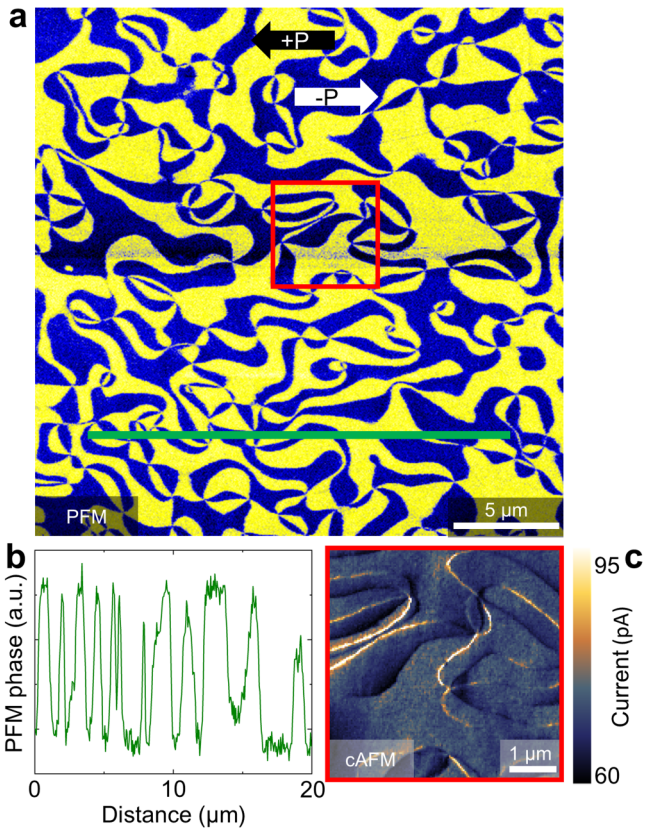

FIG. 2. (a) Calibrated in-plane PFM scan where the yellow (blue) areas represent ferroelectric polarization (P) direction pointing to the left (right). The PFM image displays a characteristic domain pattern present in hexagonal manganite single crystals, where the ferroelectric 180° domain walls meet at sixfold vertex points. (b) A representative line-profile from (a) (high values represent domains pointing to the left, *+P*; low values represent domains pointing to the right, *−P*) utilized to approximate the number of DWs per length. (c) A cAFM image from the area marked by the red box in (a). Light colors indicate areas of enhanced conductance (tail-to-tail walls), while dark areas indicate areas of lower conductance (head-to-head walls).

C. Dielectric features due to barrier layers

To disentangle surface and internal contributions, a frequency-dependent analysis of the dielectric response is required, which is shown in Fig. 3. The frequency-dependent dielectric permittivity [Fig. 3(a)] exhibits two distinct relaxations for selected temperatures varying from 170 K to 294 K. The first one in the 210 K-curve evolves at 1 kHz indicated by a step-like increase in ε' from ~20 to ~300. The lower ε'-value at high frequencies denotes the contribution of ionic and electronic polarizability to the so-called intrinsic ε_∞, confirming literature values in the order of 20–40.[18,19] The upper plateau of the second step for the 210 K-curve begins at $\nu < 100$ Hz and settles at an ε' value of the order of 5×10^3. Both relaxations are accompanied by steps in $\sigma'(\nu)$. The plateaus in σ' indicate roughly the dc-conductivity of the BLCs and the bulk. However, the dc-conductivity of step two—

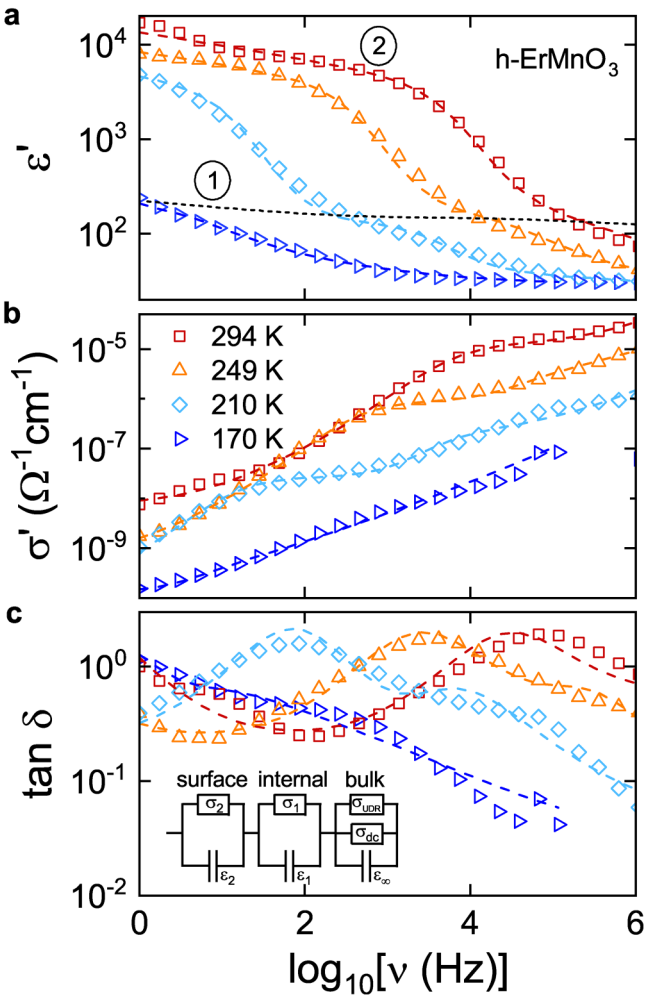

FIG. 3. Frequency-dependence of ε' (a), σ' (b), and tan δ (c) of h-$ErMnO_3$ with in-plane polarization at various temperatures (numbers ① and ② indicate the relaxation-like features; the black dashed line is a guide to the eye for the lower feature). The colored dashed lines represent fits for the measured data, obtained by considering the equivalent circuit model, sketched in the corner of (c). The equivalent circuit model consists of three *RC*-circuits connected in series.

most likely the Schottky barrier—is almost shifted out of the measured frequency range. The curvature of $\sigma'(294\,\mathrm{K})$ for $\nu < 10$ Hz indicates the onset of this dc-plateau of approximately $\sigma_{dc} \approx 3 \times 10^{-9}\,\Omega^{-1}\,\mathrm{cm}^{-1}$. The σ_{dc}-plateau of the first BLC feature emerges, e.g., for the 210 K-curve between 100 and 1000 Hz at $2 \times 10^{-8}\,\Omega^{-1}\,\mathrm{cm}^{-1}$. Finally, at higher frequencies, e.g., $\nu > 10$ kHz for 210 K-curve, σ_{dc} of the bulk evolves, which is for low temperatures superimposed by a contribution of a universal dielectric response (UDR) feature,[31] giving rise to a frequency-dependent increase in the overall conductivity.

In oxide materials, there exist different descriptions for these observed dielectric relaxation-like features: (i) hopping conductivity, (ii) displacements of DWs in excitation fields far below the coercive field, (iii) charged DWs acting as conductive inclusions,[32] (iv) Maxwell–Wagner type electrical inhomogeneities, or (v) Schottky-barriers at the electrode contacts. Hopping conductivity in disordered systems can be responsible for a continuous increase in ε' at low frequencies (typical $\nu < 1$ Hz).[1] In the present study, we observe distinct relaxation-like features strongly shifting with temperature, excluding mechanism (i). Further, the DWs are strongly pinned by the vortex structure of the hexagonal manganites and the coercive-fields for polarization reversal in h-$ErMnO_3$ are typically $> 3\,\mathrm{kV/mm}$,[19,27] which is orders of magnitude higher than the used voltage of 1 V/mm for the dielectric spectroscopy. Therefore, irreversible DW motion does not contribute to the dielectric permittivity.[33,34] In addition, the dielectric relaxation related to reversible domain wall motion typically occurs in the GHz range[35] and is temperature independent.[36] The strong temperature-dependence of the dielectric relaxation observed in our samples (Fig. 1) also allows us to exclude reversible domain wall motion as an origin. Due to these robust domain structures, mechanism (ii) seems to be very unlikely.

Interestingly, explanation model (iii) requires charged conductive DWs, which are discussed to enhance the dielectric permittivity in (K,Na)NbO_3-based ferroelectrics.[32] More specifically, a higher density of DWs leads to an increase in dielectric permittivity. Charged DWs with enhanced conductivity are also present in our samples [c.f. Fig. 2(c)]. However, in contrast to the above mentioned ferroelectric, we find the contrary behavior of the relation of DW density to the dielectric permittivity. Here, ε' decreases with increasing DW density,[17] excluding charged conductive DWs as the origin for the observed BLC feature. Thus, we focus in the following only on the latter two mechanisms of internal (iv) and surface (v) BLCs. For the present study, we investigate a single crystal, for which we can further exclude a BLC mechanism due to insulating grain boundaries, as observed in oxide ceramics.[1,12,37]

The colored dashed lines in Fig. 3 represent fits using the equivalent circuit model depicted in the inset of Fig. 3(c). This model uses the approach of Maxwell and Wagner,[38,39] for which volume fractions of the overall sample with certain capacitances and conductivities can be described by discrete *RC*-circuits connected in series. In a nutshell, we deploy *RC*-circuits for step two (surface BLC) and step one (internal BLC) in series to the bulk properties. For the latter *RC*-circuit (bulk), we use an additional frequency-dependent resistor accounting for the power-law contribution of UDR to σ'.[31] From these fits, parameters of the dielectric constants and dc-conductivities (ε'_∞, ε'_1, ε'_2, and temperature-dependent values for σ_{dc}, σ'_1, and σ'_2) are gained as listed in Table S1 in the supplementary material. The fitting parameters confirm the temperature-dependent evolution of the dielectric properties of the BLC contributions and the semiconducting behavior of the bulk.

While fitting with an equivalent circuit model allows for analyzing and disentangling single BLC contributions, it cannot provide information about the underlying mechanism. The formation of a Schottky barrier at the interface of the metal electrode and the semiconducting bulk leads to a depletion layer that acts as a thin capacitor at the sample surface. A proven approach[1,15] to establish such Schottky BLCs is to measure the dielectric

properties using electrodes of different wettings, e.g., painted vs sputtered electrodes: for Schottky BLCs, an increased wetting will provide an enhanced CDC. Further, a Schottky BLC should be strongly affected by the even small changes in the applied ac-excitation voltage.[21] Indeed, Fig. S4 in the supplementary material shows a significant impact of the ac-voltage on the dielectric properties for the surface BLC at room temperature. Internal BLCs and the intrinsic dielectric properties, however, should not be affected by these changes. Another way to prove a surface BLC is to reduce the sample thickness, as both ε' and σ' are geometry independent values, so the dielectric response should not be affected.

Figure 4 shows frequency-dependent ε' (a) and σ' (b) for both strategies indicated by different symbols (open symbols → silverpaint and d_{thick}, closed symbols → silverpaint and d_{thin}, crosses → sputtered gold and d_{thick}). Analogous to Fig. 3 both relaxations appear for the different surface treatments. Importantly, we find that the intrinsic bulk properties ③, as well as the first relaxation ① step, are—as expected for the bulk properties and an internal BLC—independent of the electrode material and the thickness of the sample. In contrast, the enhanced wetting of the sputtered electrode increases the upper plateau of ε' by a factor of about two. Furthermore, reducing the sample thickness gives rise to an increase in the CDC feature. This leads us to the conclusion that the second relaxation ② is due to the formation of an insulating depletion layer due to a Schottky barrier at the sample surface (the crossover of conductivities at low frequencies arise due to the impact of the modified surface BLCs on the accompanied relaxation-feature). Critical, and in contrast, the first relaxation is not affected by these changes to the surface, corroborating the hypothesis of an internal BLC mechanism related to insulating DWs.[17]

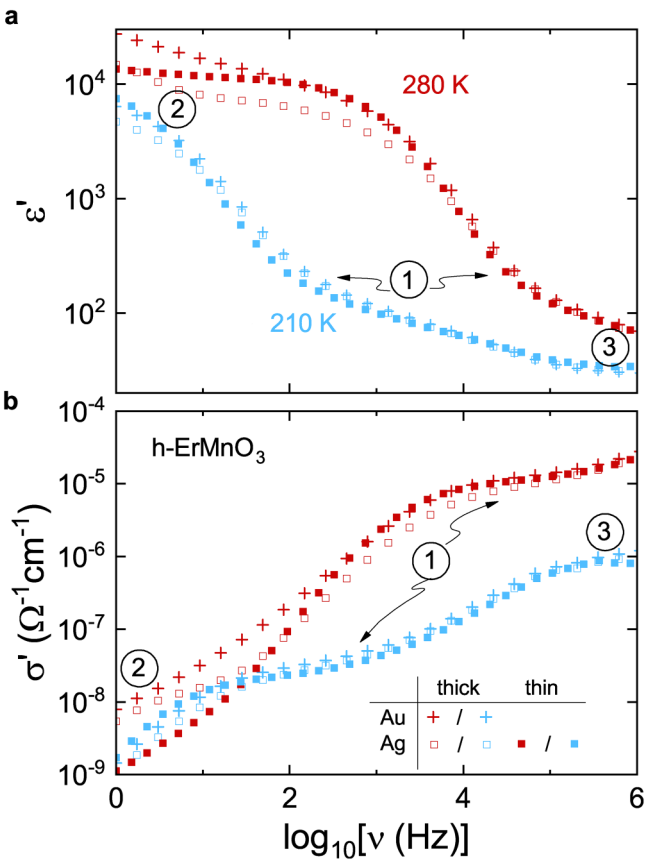

FIG. 4. Frequency-dependence of ε' (a) and σ' (b) for two representative temperatures. In this figure, the measurement data for sputtered gold and silver paint as contacting material are shown and, for the latter, also the thickness dependence ($d_{thick} = 1$ mm and $d_{thin} = 0.6$ mm). Numbers indicate the dielectric features: ①→ BLC one (internal), ②→ BLC two (surface), and ③→ bulk properties.

D. Insulating DW barrier layer capacitors

From the local-probe analysis of the sample surface (Fig. 2), in combination with bulk dielectric measurements, we calculate an approximate volume fraction (in %) of the insulating DWs in our sample: $V_{DW} = n_{DW} d_{DW}$, where n_{DW} denotes the number of insulating DWs per μm and d_{DW} the electronic thickness of the DWs referred to as electrical dressing in Meier *et al.*[22] Note that this electronic width is much larger than the structural width of about 5 Å,[40] reaching values in the order of 100–150 nm, which was related to the spreading of injected charge carriers.[22] As the contributions of the ionic and electronic polarizability to ε_∞ for both bulk and DWs are almost the same,[20] we can estimate the value of the dielectric constant ε_1. Within the framework of the Maxwell–Wagner model, ε_1 is given by the relation: $\varepsilon_1 \approx \varepsilon_\infty / V_{DW}$.

In Table I, the calculated values for the dielectric response of different samples are compared. The estimated and measured values for all samples listed in Table I are almost in the same order, providing a strong indication for a BLC-DW based mechanism. However, we note that a smeared-out relaxation due to a distribution of relaxation times of the BLC, an inhomogeneous polar pattern, as well as possible variations of the intrinsic dielectric constant cannot be excluded, adding to the uncertainty of the presented values in Table I.

Finally, we address the question, why in-plane polarized samples seem to be suited better than out-of-plane polarized specimens for detecting BLC-DW features. This can be explained employing the Maxwell–Wagner model: the relaxation-time τ_{BLC-DW} of the BLC-DW *RC*-circuit connected in series to the bulk is: $\tau_{BLC-DW} \propto \varepsilon'_1 / \sigma_{dc}$. Thus, ε'—mainly based on the number of insulating DWs and their effective thickness—and the temperature-dependent bulk σ_{dc} are strongly affecting the frequency range in which the relaxation occurs. In particular, for the samples h-$ErMnO_3$ and h-$(Er_{0.99},Ca_{0.01})MnO_3$, we measured a strongly anisotropic dc-conductivity, which is enhanced for the samples with in-plane polarization by up to a factor of 100—depending on the temperature—compared to the samples with out-of-plane polarization (Figs. S1 and S2 in the supplementary material). An enhanced dc-conductivity results in a decrease in τ_{BLC-DW} and thus in an increase in the corresponding frequency $\nu_{BLC-DW} = 1/(2\pi\tau_{BLC-DW})$. According to this, the anisotropy in the bulk σ_{dc} seems to be the most likely reason, which allows us to

TABLE I. Calculated and measured contribution of the DWs to the dielectric response for h-$RMnO_3$ (R = Y, Er) with in-plane (IP) and out-of-plane (OOP) polarization. The values are estimated from dielectric spectroscopy (Figs. 3 and S1 in the supplementary material) and local-probe analyses (Figs. 2, S2, and S3 in the supplementary material).

Sample	Dir. of P	ε_∞	n_{DW} (1/μm)	V_{DW} (%)	Estim. ε_1	Meas. ε_1
h-$ErMnO_3$ (Figs. 2, 3, and S3 in the supplementary material)	IP	32 (± 3)	0.5 (± 0.05)	7.5 (± 0.75)	400 (± 60)	250 (± 50)
h-($Er_{0.99}$, $Ca_{0.01}$)MnO_3 (Figs. S1 and S2 in the supplementary material)	IP	18	0.46	7	260	220
h-$YMnO_3$ sample 1 (data from Ruff *et al.*[17])	OOP	20	0.17	2.5	780	670
h-$YMnO_3$ sample 2 (data from Ruff *et al.*[17])	OOP	20	2.5	37.5	54	40

disentangle the contributions of surface and internal BLCs, especially in the case of samples of h-$ErMnO_3$ with in-plane polarization.

IV. SUMMARY

In this study, we investigate the contribution of insulating DWs in h-$ErMnO_3$ to the overall dielectric response up to the MHz regime. Depending on the temperature range of the dielectric measurements, two distinct relaxation-like processes are revealed, especially for samples with in-plane polarization. One of these relaxation-like features originates from a Schottky barrier, which we prove by manipulation of the sample-electrode interface. For the other feature, we conclude, corroborated by PFM and cAFM measurements, that an internal barrier layer is formed by insulating DWs. To prove this hypothesis, we first use an equivalent circuit model to quantify the bulk dielectric properties of this internal barrier layer. Second, we compare these values to a barrier layer calculated with the density and the electronic thickness of insulating DWs measured by PFM and cAFM. Based on these data, we confirm that internal barrier layer capacitors are formed at insulating DWs, which is corroborated by the comparison of different h-$YMnO_3$ and h-$ErMnO_3$ samples.

As both the density[41,42] and the electrical characteristic of the insulating DWs[18,43] can be tuned, the engineering of the macroscopic dielectric response is feasible. This may pave the way to generate high and even colossal dielectric constants by robust internal barrier layers in h-$ErMnO_3$ and h-$YMnO_3$.

SUPPLEMENTARY MATERIAL

See the supplementary material for further dielectric and local probe measurements on Ca-doped h-$ErMnO_3$, additional line scans to determine the DW density, an ac-field dependent dielectric measurement of h-$ErMnO_3$, and the fit parameters of the equivalent circuit analysis.

AUTHORS' CONTRIBUTIONS

S.K. initiated and coordinated the project. L.P. and A.S. conducted the dielectric experiments, and L.P., I.K., and S.K. analyzed the data. J.S., L.P., M.A., and D.E. performed and analyzed the local-probe experiments supervised by D.M. The single crystals were prepared by E.B. and Z.Y. All authors participated in the discussion and interpretation of the results. D.E., L.P., J.S., D.M., and S.K. wrote the manuscript.

ACKNOWLEDGMENTS

J.S. acknowledges support from the Alexander von Humboldt Foundation through the Feodor-Lynen fellowship. D.M. acknowledges support by the NTNU through the Onsager Fellowship Program and the Outstanding Academic Fellows Program, and funding from the European Research Council (ERC) under the European Union's Horizon 2020 Research and Innovation Programme (Grant Agreement No. 86691). S.K., M.A., A.S., L.P., and I.K. acknowledge funding from the German Science Foundation via the Collaborative Research Center TRR80.

DATA AVAILABILITY

The data that support the findings of this study are available from the corresponding author upon reasonable request.

REFERENCES

[1]P. Lunkenheimer, S. Krohns, S. Riegg, S. Ebbinghaus, A. Reller, and A. Loidl, Eur. J. Phys. Spec. Top. **180**, 61–89 (2009).
[2]P. Lunkenheimer, V. Bobnar, A. V. Pronin, A. I. Ritus, A. A. Volkov, and A. Loidl, Phys. Rev. B **66**, 052105 (2002).
[3]H. Kishi, Y. Mizuno, and H. Chazono, Jpn. J. Appl. Phys. **42**, 1–15 (2003).
[4]K. Hong, T. H. Lee, J. M. Suh, S.-H. Yoon, and H. W. Jang, J. Mater. Chem. C **7**, 9782–9802 (2019).
[5]J. Li, Z. Shen, X. Chen, S. Yang, W. Zhou, M. Wang, L. Wang, Q. Kou, Y. Liu, Q. Li, Z. Xu, Y. Chang, S. Zhang, and F. Li, Nat. Mater. **19**, 999–1005 (2020).
[6]J.-C. Tolédano and P. Tolédano, *The Landau Theory of Phase Transitions: Application to Structural, Incommensurate, Magnetic, and Liquid Crystal Systems*, World Scientific Lecture Notes in Physics (World Scientific, Singapore, 1987).
[7]W. J. Merz, Phys. Rev. **76**, 1221–1225 (1949).
[8]A. Devonshire, London Edinburg Dublin Philos. Mag. **40**, 1040–1063 (1949).
[9]G. Shirane, K. Suzuki, and A. Takeda, J. Phys. Soc. Jpn. **7**, 12–18 (1952).
[10]W.-B. Li, D. Zhou, L.-X. Pang, R. Xu, and H.-H. Guo, J. Mater. Chem. A **5**, 19607–19612 (2017).
[11]C. Elissalde and J. Ravez, J. Mater. Chem. **11**, 1957–1967 (2001).
[12]T. Adams, D. Sinclair, and A. West, Adv. Mater. **14**, 1321–1323 (2002).
[13]Z. Zhao, V. Buscaglia, M. Viviani, M. T. Buscaglia, L. Mitoseriu, A. Testino, M. Nygren, M. Johnsson, and P. Nanni, Phys. Rev. B **70**, 024107 (2004).
[14]M. H. Frey, Z. Xu, P. Han, and D. A. Payne, Ferroelectrics **206**, 337–353 (1998).
[15]S. Krohns, P. Lunkenheimer, S. G. Ebbinghaus, and A. Loidl, Appl. Phys. Lett. **91**, 022910 (2007).

[16]S. Krohns, P. Lunkenheimer, C. Kant, A. V. Pronin, H. B. Brom, A. A. Nugroho, M. Diantoro, and A. Loidl, Appl. Phys. Lett. **94**, 122903 (2009).
[17]E. Ruff, S. Krohns, M. Lilienblum, D. Meier, M. Fiebig, P. Lunkenheimer, and A. Loidl, Phys. Rev. Lett. **118**, 036803 (2017).
[18]T. Holstad, D. Evans, A. Ruff, D. Småbråten, J. Schaab, C. Tzschaschel, Z. Yan, E. Bourret, S. Selbach, S. Krohns, and D. Meier, Phys. Rev. B **97**, 085143 (2018).
[19]A. Ruff, Z. Li, A. Loidl, J. Schaab, M. Fiebig, A. Cano, Z. Yan, E. Bourret, J. Glaum, D. Meier, and S. Krohns, Appl. Phys. Lett. **112**, 182908 (2018).
[20]J. Schaab, S. H. Skjærvø, S. Krohns, X. Dai, M. E. Holtz, A. Cano, M. Lilienblum, Z. Yan, E. Bourret, D. A. Muller, M. Fiebig, S. M. Selbach, and D. Meier, Nat. Nanotechnol. **13**, 1028–1035 (2018).
[21]S. Krohns, P. Lunkenheimer, S. G. Ebbinghaus, and A. Loidl, J. Appl. Phys. **103**, 084107 (2008).
[22]D. Meier, J. Seidel, A. Cano, K. Delaney, Y. Kumagai, M. Mostovoy, N. A. Spaldin, R. Ramesh, and M. Fiebig, Nat. Mater. **11**, 284–288 (2012).
[23]P. Schoenherr, K. Shapovaloy, J. Schaab, Z. Yan, E. D. Bourret, M. Hentschel, M. Stengel, M. Fiebig, A. Cano, and D. Meier, Nano Lett. **19**, 1659–1664 (2019).
[24]Z. Yan, D. Meier, J. Schaab, R. Ramesh, E. Samulon, and E. Bourret, J. Cryst. Growth **409**, 75–79 (2015).
[25]C. C. Homes, T. Vogt, S. M. Shapiro, S. Wakimoto, and A. P. Ramirez, Science **293**, 673 (2001).
[26]A. B. Mosberg, E. D. Roede, D. M. Evans, T. S. Holstad, E. Bourret, Z. Yan, A. T. J. van Helvoort, and D. Meier, Appl. Phys. Lett. **115**, 122901 (2019).
[27]T. Choi, Y. Horibe, H. T. Yi, Y. J. Choi, W. Wu, and S. W. Cheong, Nat. Mater. **9**, 253–258 (2010).
[28]T. Jungk, A. Hoffmann, M. Fiebig, and E. Soergel, Appl. Phys. Lett. **97**, 012904 (2010).
[29]M. Safrankova, J. Fousek, and S. Kiazev, Czech. J. Phys. **17**, 559 (1967).
[30]A. Hubert and R. Schäfer, *Magnetic Domains* (Springer-Verlag, Berlin, 1998).
[31]A. Jonscher, Nature **267**, 673–679 (1977).
[32]A. A. Esin, D. O. Alikin, A. P. Turygin, A. S. Abramov, J. Hreščak, J. Walker, T. Rojac, A. Bencan, B. Malic, A. L. Kholkin, and V. Y. Shur, J. Appl. Phys. **121**, 074101 (2017).
[33]B. Lewis, Proc. Phys. Soc. **73**, 17 (1959).
[34]D. A. Hall and P. J. Stevenson, Ferroelectrics **228**, 139 (1999).
[35]C. Kittel, Phys. Rev. Lett. **83**, 458 (1951).
[36]G. Arlt, U. Böttger, and S. Witte, Ann. Phys. **506**, 578 (1994).
[37]A. J. Moulson and J. M. Herbert, *Electroceramics* (John Wiley & Sons, Ltd, 2003), Chap. 5, pp. 243–337.
[38]K. W. Wagner, Arch. Elektrotech. **2**, 371–387 (1914).
[39]J. C. Maxwell, *A Treatise on Electricity and Magnetism* (Clarendon Press, Oxford, 1873).
[40]M. E. Holtz, K. Shapovalov, J. A. Mundy, C. S. Chang, Z. Yan, E. Bourret, D. A. Muller, D. Meier, and A. Cano, Nano Lett. **17**, 5883–5890 (2017).
[41]Q. N. Meier, M. Lilienblum, S. M. Griffin, K. Conder, E. Pomjakushina, Z. Yan, E. Bourret, D. Meier, F. Lichtenberg, E. K. H. Salje, N. A. Spaldin, M. Fiebig, and A. Cano, Phys. Rev. X **7**, 041014 (2017).
[42]S. M. Griffin, M. Lilienblum, K. T. Delaney, Y. Kumagai, M. Fiebig, and N. A. Spaldin, Phys. Rev. X **2**, 041022 (2012).
[43]E. Hassanpour, V. Wegmayr, J. Schaab, Z. Yan, E. Bourret, T. Lottermoser, M. Fiebig, and D. Meier, New J. Phys. **18**, 043015 (2016).